

Acoustic radiation force on a rigid cylinder near rigid corner boundaries exerted by a Gaussian beam field

Qin Chang(常钦), Yuchen Zang(臧雨宸), Weijun Lin(林伟军), Chang Su(苏畅), and Pengfei Wu(吴鹏飞)
Citation: Chin. Phys. B, 2022, 31 (**4**): 044302. DOI: 10.1088/1674-1056/ac2d1f
Journal homepage: http://cpb.iphy.ac.cn; http://iopscience.iop.org/cpb

What follows is a list of articles you may be interested in

Rotational manipulation of massive particles in a 2D acoustofluidic chamber constituted by multiple nonlinear vibration sources

Qiang Tang(汤强), Pengzhan Liu(刘鹏展), and Shuai Tang(唐帅)
Chin. Phys. B, 2022, 31 (**4**): 044301. DOI: 10.1088/1674-1056/ac1f0e

Weak-focused acoustic vortex generated by a focused ring array of planar transducers and its application in large-scale rotational object manipulation

Yuzhi Li(李禹志), Peixia Li(李培霞), Ning Ding(丁宁), Gepu Guo(郭各朴), Qingyu Ma(马青玉), Juan Tu(屠娟), and Dong Zhang(章东)
Chin. Phys. B, 2021, 30 (**4**): 044302. DOI: 10.1088/1674-1056/abca1f

Axial acoustic radiation force on an elastic spherical shell near an impedance boundary for zero-order quasi-Bessel-Gauss beam

Yu-Chen Zang(臧雨宸), Wei-Jun Lin(林伟军), Chang Su(苏畅), and Peng-Fei Wu(吴鹏飞)
Chin. Phys. B, 2021, 30 (**4**): 044301. DOI: 10.1088/1674-1056/abca27

Acoustic radiation force on thin elastic shells in liquid

Run-Yang Mo(莫润阳), Jing Hu(胡静), Shi Chen(陈时), Cheng-Hui Wang(王成会)
Chin. Phys. B, 2020, 29 (**9**): 094301. DOI: 10.1088/1674-1056/ab943e

Pulling force of acoustic-vortex beams on centered elastic spheres based on the annular transducer model

Yuzhi Li(李禹志), Qingdong Wang(王青东), Gepu Guo(郭各朴), Hongyan Chu(褚红燕), Qingyu Ma(马青玉), Juan Tu(屠娟), Dong Zhang(章东)
Chin. Phys. B, 2020, 29 (**5**): 054302. DOI: 10.1088/1674-1056/ab8210

Acoustic radiation force on a rigid cylinder near rigid corner boundaries exerted by a Gaussian beam field

Qin Chang(常钦)[1,2], Yuchen Zang(臧雨宸)[1,2], Weijun Lin(林伟军)[1,2,3,†], Chang Su(苏畅)[1,2,3], and Pengfei Wu(吴鹏飞)[1,2,3]

[1] *Institute of Acoustics, Chinese Academy of Sciences, Beijing* 100190, *China*
[2] *University of Chinese Academy of Sciences, Beijing* 100049, *China*
[3] *Beijing Deep Sea Drilling Measurement Engineering Technology Research Center, Beijing* 100190, *China*

(Received 1 August 2021; revised manuscript received 17 September 2021; accepted manuscript online 6 October 2021)

Acoustic manipulation is one of the well-known technologies of particle control and a top research in acoustic field. Calculation of acoustic radiation force on a particle nearby boundaries is one of the critical tasks, as it approximates realistic applications. Nevertheless, it is quite difficult to solve the problem by theoretical method when the boundary conditions are intricate. In this study, we present a finite element method numerical model for the acoustic radiation force exerting on a rigid cylindrical particle immersed in fluid near a rigid corner. The effects of the boundaries on acoustic radiation force of a rigid cylinder are analyzed with particular emphasis on the non-dimensional frequency and the distance from the center of cylinder to each boundary. The results reveal that these parameters play important roles in acoustic manipulation for particle-nearby complicated rigid boundaries. This study verifies the feasibility of numerical analysis on the issue of acoustic radiation force calculation close to complex boundaries, which may provide a new idea on analyzing the acoustic particle manipulation in confined space.

Keywords: acoustic radiation force, finite element method, Gaussian beam field, acoustic manipulation

PACS: 43.25.Qp, 43.35.Wa, 43.80.Gx **DOI:** 10.1088/1674-1056/ac2d1f

1. Introduction

As the fundamentals in biomedical ultrasound, material science and other fields, acoustic radiation force has become hotspots in acoustic tweezers,[1,2] and acoustic levitation,[3] etc. Since King[4] first proposed the concept of acoustic radiation force for particles and figured out an analytical expression for the acoustic radiation force of a rigid sphere in the ideal fluid in 1934, scholars have developed many models to describe the acoustic radiation force of the particles in various acoustic fields.[5–21] In earlier researches, particles were usually defined as ideal geometries (cylinders or spheres) with simple solid mechanical properties (rigid or elastic) and these particles were commonly supposed to be suspended in a free acoustic field. However, in many practical applications, the walls of the container are more diverse and ignoring the influence will cause errors. For example, a round-bottomed flask can be regarded as a combination of two: a sphere and a cylinder, and the connection between two parts can be treated as a transition from a cylinder to a sphere. If researchers intend to solve the acoustic radiation force on a particle moved from the bottom of the flask to the top, the calculation will be difficult but critical when the particle goes through the connection. Therefore, researchers tried to study effects of the boundaries on the acoustic radiation force.

In 1994, Guanauard[22] calculated the acoustic scattering of a sphere near a plane boundary firstly. Later, Huang and Guanauard[23] computed the scattering of a plane acoustic wave by a spherical elastic shell near a free surface. On the basis of Guanauard's research, Miri *et al.*[24] analyzed the effect of a porous wall on the acoustic radiation force for contrast agent shells in detail. Wang *et al.*[25] theoretically and numerically studied the acoustic radiation force exerted by a standing wave on a rigid cylinder near a flat wall. Qiao *et al.*[26–30] systematically studied the acoustic radiation force on cylindrical particles near an impedance boundary for both plane waves and Gaussian beam fields. More recently, our group extended Qiao's results to the case for a 3D spherical shell near the interface.[31]

In fact, for the limitation of calculation method, it is hard to process transmission and reflection between particles and complex boundaries manually. However, benefiting from the development of analysis software, utilizing the computer to compute the acoustic radiation force via simulating the scattering sound field seems to be an effective method. In this investigation, a 2-D acoustic model is built by a finite element method (FEM) software and most of the calculations are performed by computer. In this model, there is a rigid corner boundary and a rigid cylindrical particle near the boundary in a Gaussian beam field. The spatial positions of geometries are adjustable, such as the angle between two rigid boundaries and the distances between particle and boundaries. In addition, particular emphases are paid to the beam frequency, the

[†]Corresponding author. E-mail: linwj@mail.ioa.ac.cn

© 2022 Chinese Physical Society and IOP Publishing Ltd

incidence angle, and the beam waist radius. It is convenient to study the effects of boundaries on the acoustic radiation force by changing the parameters. On the basis of studies on the rigid corner case, a demonstration of calculating the acoustic radiation force exerting on a rigid cylindrical particle immersed in fluid near a rigid circular corner is briefly introduced to verify the universality of the FEM model.

2. Method

2.1. Theoretical analyses

As shown in Fig. 1, a corner is full of fluid with two rigid boundaries forming an angle α. A rigid cylindrical particle immersed in the fluid is perpendicular to the X–O–Y plane near by the corner, d_1 and d_2 represent the distance from the central of particle to boundary 1 and boundary 2, respectively. A weakly focused Gaussian beam field is incident upon the particle, where φ represents the angle between the beam axis and the X-direction.

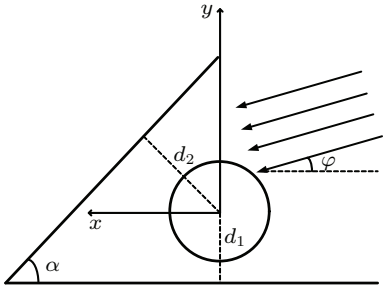


Fig. 1. The 2D acoustic model used to calculate the acoustic radiation force on a rigid cylindrical particle near a rigid corner immersed in water.

2.2. Theoretical analyses in the case of right angle

Partial wave series expansion method (PWSEM) is a classical method to analyze the acoustic radiation force. When the two flat boundaries form a right corner, it is convenient to deal with the problem analytically based on the image method. Three image cylinders are placed at the symmetrical positions to equate the effects of boundaries. The incident wave in the jth coordinate system is expressed in the coordinate system of the pth cylinder as

$$\phi_{\text{inc}}^{(jp)} = \phi_0 \, \mathrm{e}^{-\mathrm{i}\omega t} \sum_{n=-\infty}^{\infty} \gamma_n^{(jp)} J_n(kr_p) \, \mathrm{e}^{\mathrm{i}n\theta_p}. \tag{1}$$

Here, ϕ_0 is the amplitude of velocity potential, $k = \omega/c$ is the wave number with c being the sound speed in the host fluid, ω is the angular frequency, and J_n is the nth-order cylindrical Bessel function. The detailed expression of $\gamma_n^{(jp)}$ is

$$\gamma_n^{(jp)} = \mathrm{i}^n \, \mathrm{e}^{-\mathrm{i}n\beta_j} \, \mathrm{e}^{\mathrm{i}kl_{jp}\cos(\beta_j - \theta_{jp})}, \tag{2}$$

where $\beta_1 = \pi + \varphi$, $\beta_2 = -\varphi$, $\beta_3 = \varphi$, $\beta_4 = \pi - \varphi$, $l_{jp} = l_{pj}$ $(j, p = 1, 2, 3, 4)$, $l_{12} = l_{34} = 2(a + d_1)$, $l_{14} = l_{23} = 2(a + d_2)$ and $l_{jp} = 0$ if $j = p$.

The scattering velocity potential can also be expressed as

$$\phi_{\text{sca}}^{(p)} = \phi_0 \, \mathrm{e}^{-\mathrm{i}\omega t} \sum_{n=-\infty}^{\infty} C_n^{(p)} H_n^{(1)}(kr_p) \, \mathrm{e}^{\mathrm{i}n\theta_p}, \tag{3}$$

where $H_n^{(1)}$ is the nth-order cylindrical Hankel function of the first kind, $C_n^{(p)}$ represents the scattering expansion coefficients determined by applying appropriate boundary conditions at the surface.

The translational addition theorem for cylindrical functions is applied here to write all the wave fields in the same coordinate system, which is given by

$$\begin{aligned} &H_n^{(1)}(kr_p) \, \mathrm{e}^{\mathrm{i}n\theta_p} \\ &= \sum_{m=-\infty}^{\infty} J_m(kr_j) H_{n-m}^{(1)}(kl_{pj}) \, \mathrm{e}^{\mathrm{i}(n-m)\theta_{pj} + \mathrm{i}m\theta_j}. \end{aligned} \tag{4}$$

Hereafter, the total velocity potential is obtained as

$$\phi_{\text{tot}} = \phi_{\text{sca}}^{(p)} + \sum_{j=1}^{4} \left[\phi_{\text{inc}}^{(jp)} + (1 - \delta_{jp}) \phi_{\text{sca}}^{(jp)} \right], \tag{5}$$

where δ_{jp} is the Kronecker delta function.

For an absolutely rigid cylinder, the normal component velocity must vanish at the surface of the cylinder. Applying this boundary condition leads to

$$\sum_{j=1}^{4} \left[C_n^{(p)} \delta_{jp} - (1 - \delta_{jp}) D_{nm}^{(jp)} C_n^r \right] = C_n^r \sum_{j=1}^{4} \gamma_n^{(jp)}, \tag{6}$$

where

$$\begin{aligned} C_n^r &= -J_n'(ka) / H_n^{(1)\prime}(ka), \\ D_{nm}^{(jp)} &= \sum_{m=-\infty}^{\infty} C_m^{(j)} H_{m-n}^{(1)}(kl_{jp}) \, \mathrm{e}^{\mathrm{i}(m-n)\theta_{jp}}. \end{aligned}$$

An object will experience a mean force, known as acoustic radiation force, when subjected to a harmonic-continuous sound field. Considering that the surrounding fluid is ideal and cannot absorb any momentum from the sound wave, the acoustic radiation force can be computed by integrating the radiation stress tensor over a circular cylindrical surface S_0 enclosing the cylinder. It has been proved to be advantageous to evaluate the radiation force using the far-field scattering, which can be expressed as[32]

$$\begin{aligned} &\langle \boldsymbol{F} \rangle_{kr \to \infty} \\ &= \frac{1}{2} \rho_0 k^2 \iint_{S_0} \mathrm{Re} \left[\phi_{\text{sca}}^* \left(\frac{\mathrm{i}}{k} \frac{\partial \phi_{\text{inc}}}{\partial r} - \phi_{\text{inc}} - \phi_{\text{sca}} \right) \right] \mathrm{d}\boldsymbol{S}, \end{aligned} \tag{7}$$

where $\mathrm{d}\boldsymbol{S} = \mathrm{d}S\boldsymbol{e}_r$ with $\mathrm{d}S = Lr\mathrm{d}\theta$ being the scalar differential element of a cylindrical surface S in length L taken at a large radius r enclosing the cylinder, the outward unit vector is $\boldsymbol{e}_r = \cos\theta \boldsymbol{e}_x + \sin\theta \boldsymbol{e}_y$, with $\boldsymbol{e}_x$ and $\boldsymbol{e}_y$ being the unit vectors in the coordinate system xOy, Re denotes the real part of a complex function, the superscript * denotes the complex conjugate of a complex function, and the symbol $\langle\ \rangle$ represents time averaging.

Projecting Eq. (7) into the x and y axes, we can obtain the expression of the two component radiation forces, respectively, as

$$\begin{Bmatrix} F_x \\ F_y \end{Bmatrix} = \langle \boldsymbol{F} \rangle \cdot \begin{Bmatrix} \boldsymbol{e}_x \\ \boldsymbol{e}_y \end{Bmatrix} = \begin{Bmatrix} Y_x \\ Y_y \end{Bmatrix} S_c E_0, \tag{8}$$

where $S_c = 2aL$ is the surface cross section of the cylinder, $E_0 = \rho k^2 \phi_0^2/2$ is the characteristic energy density, the dimensionless factors Y_x and Y_y are the two components of the acoustic radiation force function, which represent the radiation force per unit energy density and unit cross-sectional surface. Their expressions are given by

$$Y_x = \frac{1}{ka} \mathrm{Im} \left\{ \sum_{n=-\infty}^{+\infty} \left[\sum_{j=1}^{4} \left(\gamma_n^{j1} + (1-\delta_{j1}) D_{nm}^{(j1)} \right) + C_n^{(1)} \right] \times \left(C_{n+1}^{(1)*} - C_{n-1}^{(1)*} \right) \right\}, \tag{9}$$

$$Y_x = -\frac{1}{ka} \mathrm{Im} \left\{ \sum_{n=-\infty}^{+\infty} \left[\sum_{j=1}^{4} \left(\gamma_n^{j1} + (1-\delta_{j1}) D_{nm}^{(j1)} \right) + C_n^{(1)} \right] \times \left(C_{n+1}^{(1)*} + C_{n-1}^{(1)*} \right) \right\}, \tag{10}$$

where Im denotes the imaginary part of a complex function.

2.3. Numerical model

Based on the simplification from the tensor integral approach, Y_x and Y_y are defined as

$$\langle \boldsymbol{F} \rangle = -\left\langle \oint\!\!\oint_0 \rho_0 (v_n \boldsymbol{n} + v_t \boldsymbol{t}) v_n \boldsymbol{n} \, \mathrm{d}l \right\rangle + \left\langle \oint\!\!\oint_{l_0} \frac{\rho_0}{2} |v|^2 \boldsymbol{n} \, \mathrm{d}l \right\rangle - \left\langle \oint\!\!\oint_{l_0} \frac{\rho_0}{2c_0^2} \dot{\phi}^2 \boldsymbol{n} \, \mathrm{d}l \right\rangle, \tag{11}$$

$$\langle \boldsymbol{F}_{x,y} \rangle = \boldsymbol{Y}_{x,y} I, \tag{12}$$

$$\boldsymbol{n} = (n_x, n_y), \tag{13}$$

$$Y_x = \frac{1}{I} \sum_{l_0} \left[-\langle \rho_0 (v_x n_x + v_y n_y) v_x^* \rangle + \left\langle \frac{\rho_0}{2} (v_x \cdot v_x^* + v_y \cdot v_y^*) n_x \right\rangle - \left\langle \frac{1}{2c_0^2} p \cdot p^* \cdot n_x \right\rangle \right] \Delta l, \tag{14}$$

$$Y_y = \frac{1}{I} \sum_{l_0} \left[-\langle \rho_0 (v_x n_x + v_y n_y) v_y^* \rangle + \left\langle \frac{\rho_0}{2} (v_x \cdot v_x^* + v_y \cdot v_y^*) n_y \right\rangle - \left\langle \frac{1}{2c_0^2} p \cdot p^* \cdot n_y \right\rangle \right] \Delta l. \tag{15}$$

The values of Y_x and Y_y can be calculated by Eq. (14) and (15), if the parameters of medium and the scattering sound field are known.

In this study, the acoustic pressure and particle velocity distributions in the fluid medium are calculated by COMSOL Multiphysics (version 5.6, COMSOL AB, Stockholm, Sweden). COMSOL is one of the most commonly used FEM software in acoustics, optics, electromagnetics, mechanics and other relevant fields. In the acoustics module (Pressure Acoustics, Frequency Domain) of COMSOL, the total acoustic pressure field P_t is caused by the superposition of background pressure field P_b and scattered acoustic pressure field P_s, and the total velocity is described by its root-mean-square value v_{rms}. The acoustic radiation force is considered to be induced by acoustic scattering, which is due to the momentum transfer between the acoustic wave and the particle. P_s and v_{rms} are calculated by computer. P_b is the external incident Gaussian beam field.

As shown in Fig. 2, the calculated domain is comprised of a fluid domain and a perfectly matched layer (PML) domain. The PML domain is used to absorb the acoustic waves at the edge of the fluid domain. The corresponding parameters are clearly listed in Table 1. Especially, the radius of scatterer particle a is a constant in this research.

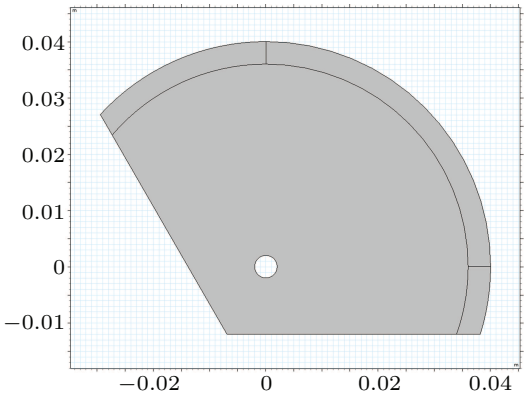


Fig. 2. The FEM model used to calculate the acoustic radiation force on a rigid cylindrical particle near a rigid corner immersed in water.

Table 1. Parameters used for the simulation.

Symbol	Description	Value
f_0	maximum frequency	1.2 MHz
f	frequency	$0.01 f_0$–f_0
c_0	speed of sound in air	1494 m/s
λ	wavelength in water	c_0/f
W	radius of beam waist	3λ–10λ
w	normalized radius of beam waist, $w = W/\lambda$	3–10
ρ_0	density of water	1000 kg/m^3
a	radius of scatterer particle	2.00 mm
D_1	distance from the central of particle to rigid boundary 1	4.00–20.00 mm
D_2	distance from the central of particle to rigid boundary 2	4.00–20.00 mm
d_1	normalized distance D_1, $d_1 = D_1/a$	2–10
d_2	normalized distance D_2, $d_2 = D_2/a$	2–10
α	angle between two rigid boundaries	30°–120°
φ	incident angle of Gaussian beam field	0°–180°

After executing the Mesh module, the geometry is divided into plenty of area elements and then computer will process the model on the basis of meshes by execute the Study module. Figures 3 and 4 show the meshes and the total acoustic pres-

sure field of a sample generated by COMSOL. In this sample, $f = 1.2$ MHz, $w = 3$, $\alpha = 120°$, $\varphi = 60°$, and $d_1 = d_2 = 6$.

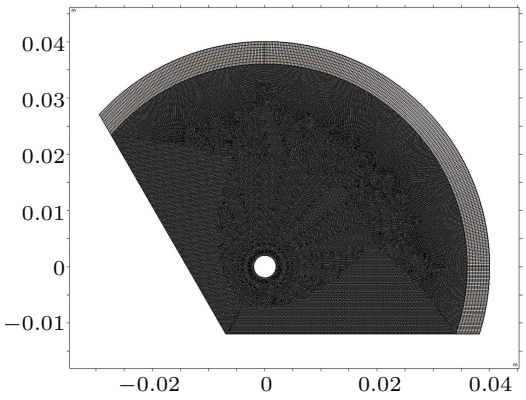


Fig. 3. The meshes for the sample divided by COMSOL.

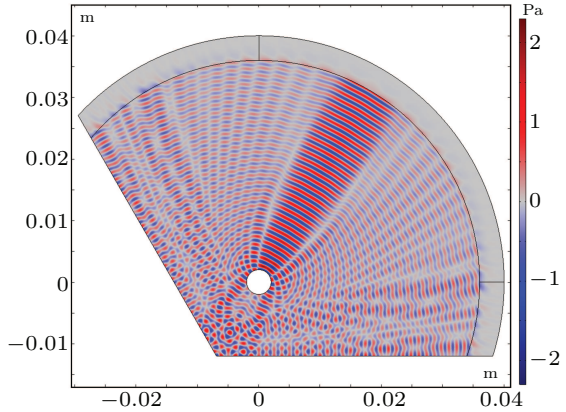


Fig. 4. The total acoustic pressure field P_t for the sample calculate by COMSOL.

3. Numerical calculations and analyses

The axial acoustic radiation force function component Y_p on a rigid cylinder in free space exerted by a plane wave is one of the most classical model and the results have been verified by many researchers. A comparison between the theoretical results of PWSEM and the numerical results of FEM to figure out the accuracy of the numerical model is shown in Fig. 5. The maximum absolute error is 0.0229 and the correlation coefficient between PWSEM and FEM is 0.9994, which can verify the reliability of the FEM model.

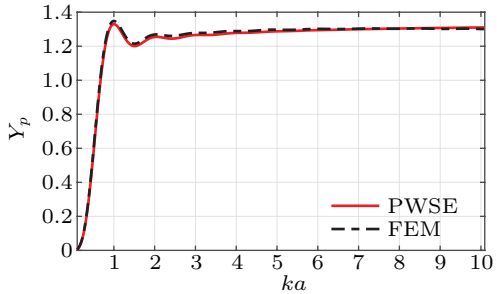


Fig. 5. The axial acoustic radiation force function component Y_p on a rigid cylinder in free space exerted by a plane wave.

In theoretical researches, the 2D Gaussian beam field is defined as

$$P = P_0 \mathrm{e}^{-\frac{y^2}{W}} \mathrm{e}^{-\mathrm{i}kx}. \tag{16}$$

It is worth noting that a weakly focused Gaussian beam field emitted from a transducer cannot be described by Eq. (16) because the phase variety is ignored. In this case, the weakly focused Gaussian beam field only remains a half as shown in Fig. 6.

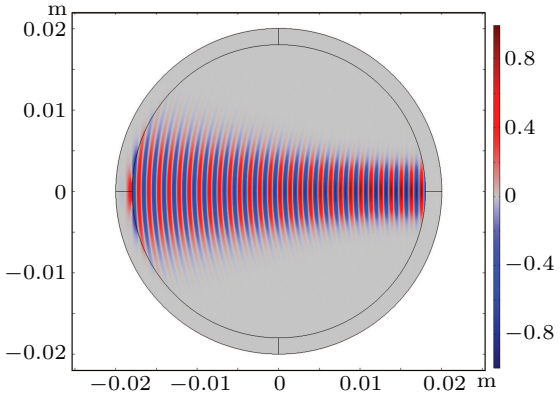


Fig. 6. A phase-ignored weakly focused Gaussian beam field simulated by COMSOL.

In this investigation, the weakly focused Gaussian beam field is considered to be back to the original 2D Gaussian beam in optics:

$$P = P_0 \mathrm{e}^{-\frac{y^2}{W(x)}} \mathrm{e}^{-\mathrm{i}\left[k\left(x+\frac{y^2}{2R(x)}\right)-\arctan\frac{z}{x_\mathrm{R}}\right]}, \tag{17}$$

$$W(x) = W_0\sqrt{1+\left(\frac{x}{x_\mathrm{R}}\right)^2}, \tag{18}$$

$$R(x) = x + \frac{x_\mathrm{R}^2}{x}, \tag{19}$$

$$x_\mathrm{R} = \frac{\pi W_0^2}{\lambda}, \tag{20}$$

where $W(x)$ is the Rayleigh radius in optics that is often substituted by the radius of beam waist W_0 in acoustics, x_R is the Rayleigh range, and $R(x)$ is curvature radius. The relationship of these parameters is shown in the Fig. 7. Equation (17) is confirmed to be more realistic than Eq. (16) because the Gaussian beam field defined by Eq. (17) can describe the complete Gaussian beam field correctly. The correct Gaussian beam field is shown in Fig. 8.

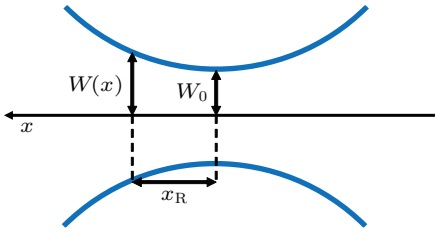


Fig. 7. An optical Gaussian beam.

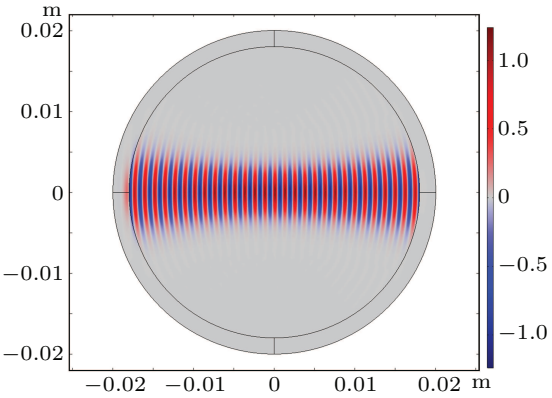


Fig. 8. An optical Gaussian beam.

Because of the different expressions of Gaussian beam field, it is necessary to check the applicability of Eq. (17). The result of the axial acoustic radiation force function component Y_p on a rigid cylinder in free space exerted by an optical Gaussian beam is shown in Fig. 9. When ka increases, Y_p decrease as a increases. However, according to the results of PWSEM studied by many researchers, if the ka is defined, there will be no direct relation between Y_p and a. This phenomenon suggests that Eqs. (16) and (17) are approximate only in a certain range ($a = 2$–3 mm). In this research, a is finally set as 2.00 mm for the comparison with the theoretical results from other studies.

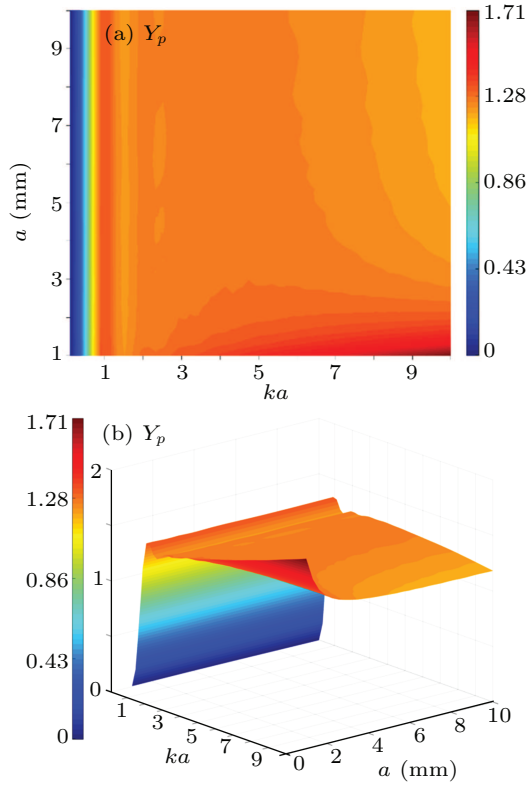


Fig. 9. The axial acoustic radiation force function component Y_p versus a and ka for a rigid cylindrical in free space exerted by an optical Gaussian beam field. (a) The 2D plots of Y_p. (b) The 3D plots of Y_p, with $ka = 10$.

Varying the values of w and ka, the simulated results of the axial acoustic radiation force functions Y_x and Y_y are shown in Fig. 10. It is shown that Y_x and Y_y are both constant when ka is lower than 6. However, if ka is larger than 6, Y_x and Y_y decrease with increasing w. The results suggest that the axial acoustic radiation force is affected by the ratio of a to λ. Only when the radius of particle is large enough (the ratio is large enough), Y_x and Y_y are sensitive to the variation of w.

It is particular to note that all of the color bars in these figures are set symmetric about zero to make the positive values red and the negative values blue, which makes it easier for readers to distinguish the positive and negative values.

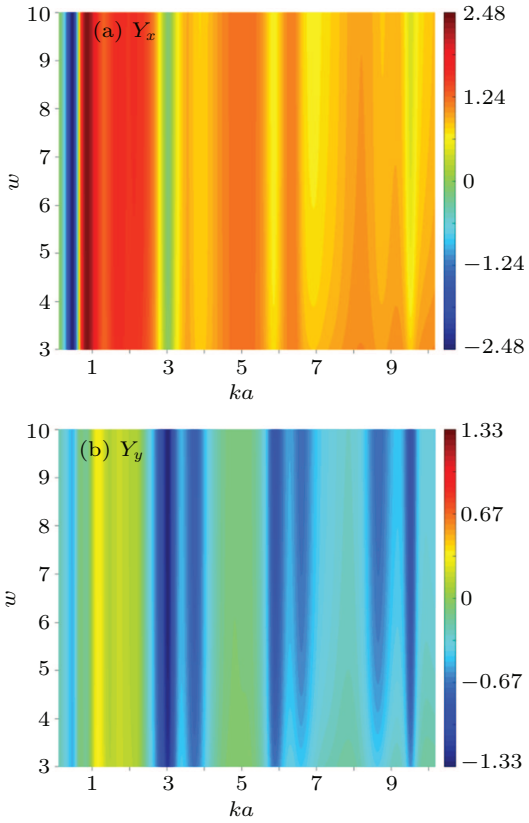


Fig. 10. The 2D plots of the acoustic radiation force function components versus ka and w for a rigid cylindrical particle near a rigid corner placed in a Gaussian beam field. The angle α between two rigid boundaries is set as 120°, the incident angle φ is set as 0° and the normalized distance $d_1 = d_2 = 2$. (a) The acoustic radiation force component in the X direction. (b) The acoustic radiation force component in the Y direction.

Figure 11 plots the axial radiation force functions Y_x and Y_y versus the normalized distances d_1 and d_2. It is found that Y_x and Y_y varies periodically along with the change of d_2 at a certain d_1 value. However, the amplitudes of the Y_x and Y_y peaks decrease with the increase of d_1 when the value of d_1 is around from 2 to 5; when d_1 is more than 5, the amplitudes of Y_x and Y_y are stable. Switching d_1 and d_2 will lead to the analogous results.

The regular patterns verify that Y_x and Y_y are influenced by the standing wave existing between rigid boundaries and the surface of particle. As the distances d_1 and d_2 change, Y_x and Y_y will be enhanced or weaken frequently when they meet the conditions of the standing wave. In addition, it shows that

the positions of the maximal values are identical whereas the values are opposite. This phenomenon is due to the fact that Y_x and Y_y are two components of the acoustic radiation force. If each one becomes the maximum, the other must be minimal.

It is noteworthy that there exists the negative acoustic radiation force at selected d_1 and d_2 values, where the backscattering of the sphere is suppressed.

All the parameters are kept the same as those in Figs. 11(a) and 11(b) except ka ($ka = 1$) and the results are shown in Figs. 11(c)–11(f). Since the value of ka is smaller in this case, the details of transformation tendency of the acoustic radiation force function in large wavelength are clearer. Considering that d_2 ranges from 2 to 7, Y_x and Y_y are more sensitive to the variation of d_1 and it can be observed that the transformation frequency of acoustic radiation force tends to be higher as d_2 becomes smaller. If ka is smaller ($ka = 0.5$), the phenomenon is more obvious as shown in Figs. 11(e) and 11(f). Combined with the conclusions $ka = 3$, the increase of d_2 does not influence the transformation frequency when d_2 increases so as to generate the third peak. In addition, negative acoustic radiation force is also found, in that case the backscattering acoustic scattering is suppressed.

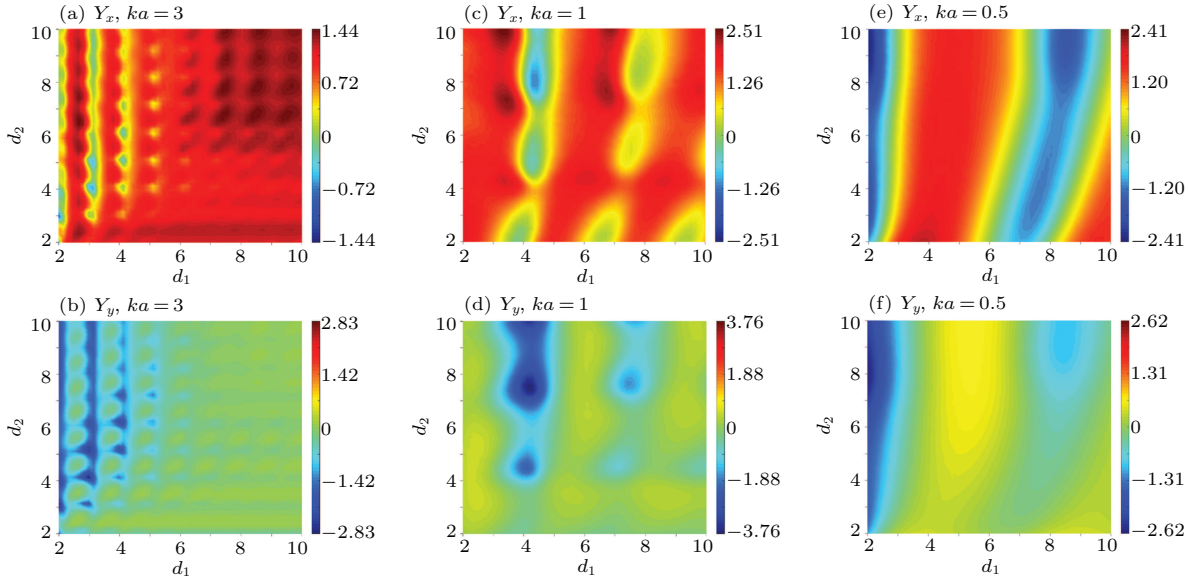


Fig. 11. The 2D plots of the acoustic radiation force function components versus d_1 and d_2 for a rigid cylindrical particle near a rigid corner placed in a Gaussian beam field. The angle α between two rigid boundaries is set as 120°, the incident angle φ is set as 0° and the beam waist w is set as 3. [(a), (c), (d)] The acoustic radiation force component in the X direction. [(b), (d), (f)] The acoustic radiation force component in the Y direction. In (a), (b), (c), (d), (e) and (f), the ka is set as 3, 3, 1, 1, 0.5 and 0.5, respectively.

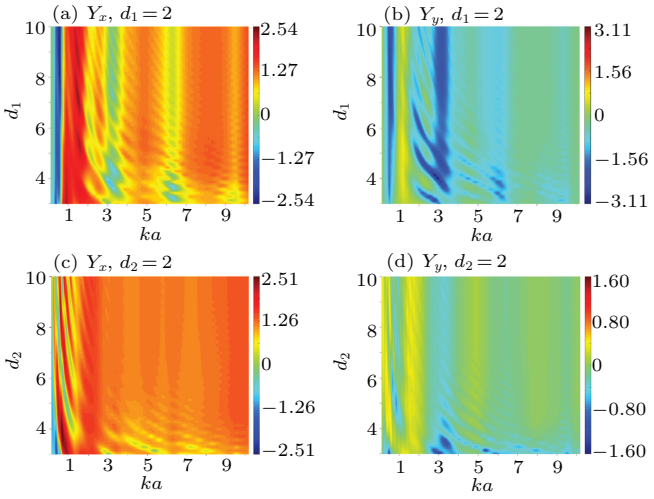


Fig. 12. The 2D plots of the acoustic radiation force function components versus ka and each normalized distances for a rigid cylindrical particle near a rigid corner placed in a Gaussian beam field. The angle α between two rigid boundaries is set as 120°, the incident angle φ is set as 0° and the normalized radius of beam waist w is set as 3. [(a), (c)] The acoustic radiation force component in the X direction. [(b), (d)] The acoustic radiation force component in the Y direction. [(a), (b)] The d_2 is set as 2. [(c), (d)] The d_1 is set as 2.

According to the results in Fig. 12, the values of d_1 and d_2 are varied independently to figure out the relationship between the normalized distance and ka. It is similar to Fig. 10, when the normalized wavelength is larger than particle radius (ka is small enough), Y_x and Y_y are insensitive to d_1 or d_2. However, as ka increases, Y_x and Y_y exhibit periodical variations along with d_1 or d_2 and there is a positive correlation between the beam frequency and ka. All of the above phenomena are also caused by the standing wave. When ka is fixed, the quantity of peaks will increase with the increase of d_1 or d_2, and vice versa.

In real applications, the angle between two boundaries and the incident angle are often varied to meet different demands. Figure 13 predicts the 2D plots of the acoustic radiation force function components versus ka and α for a rigid cylindrical particle near a rigid corner placed in a Gaussian beam field. The incident wave is set to be in parallel to the X axis, and the normalized radius of beam waist w is set as 3. Figure 14 shows the corresponding plots for the radiation force functions versus ka and ϕ at $\alpha = 120°$ and $w = 3$. The maximal and minimal values of the acoustic radiation force

function can be easily observed in the simulated plots.

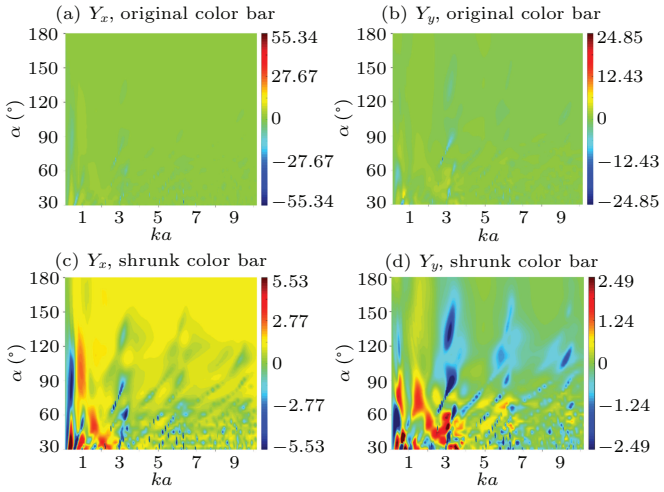


Fig. 13. The 2D plots of the acoustic radiation force function components versus ka and α for a rigid cylindrical particle near a rigid corner placed in a Gaussian beam field. The incident angle φ is set as 0°, and the normalized radius of beam waist w is set as 3. [(a), (c)] The acoustic radiation force component in the X direction. [(b), (d)] The acoustic radiation force component in the Y direction. In (a) and (b), the color bar is original. In (c) and (d), the color bar is shrunk to one tenth of the original.

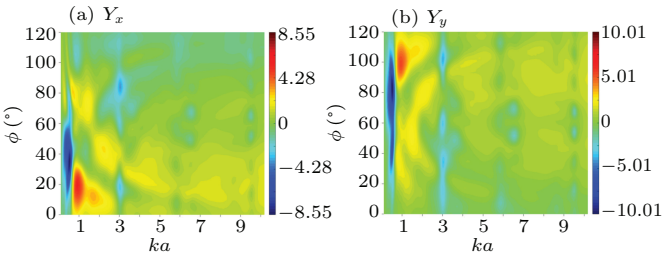


Fig. 14. The 2D plots of the acoustic radiation force function components versus ka and φ for a rigid cylindrical particle near a rigid corner placed in a Gaussian beam field. The angle α between two rigid boundaries is set as 120°, and the normalized distance $d_1 = d_2 = 2$. (a) The acoustic radiation force component in the X direction. (b) The acoustic radiation force component in the Y direction.

On the basis of the results of the rigid corner case, it is convenient to calculate the acoustic radiation force function on a particle nearby arbitrary boundaries. An example is given here to demonstrate the calculation of the acoustic radiation force function on a rigid cylindrical particle nearby a circular rigid corner, in which the curvature radius of circular corner is set as $2a$. The comparison between the numerical models for a right angle rigid corner and a circular rigid corner is shown in Fig. 15.

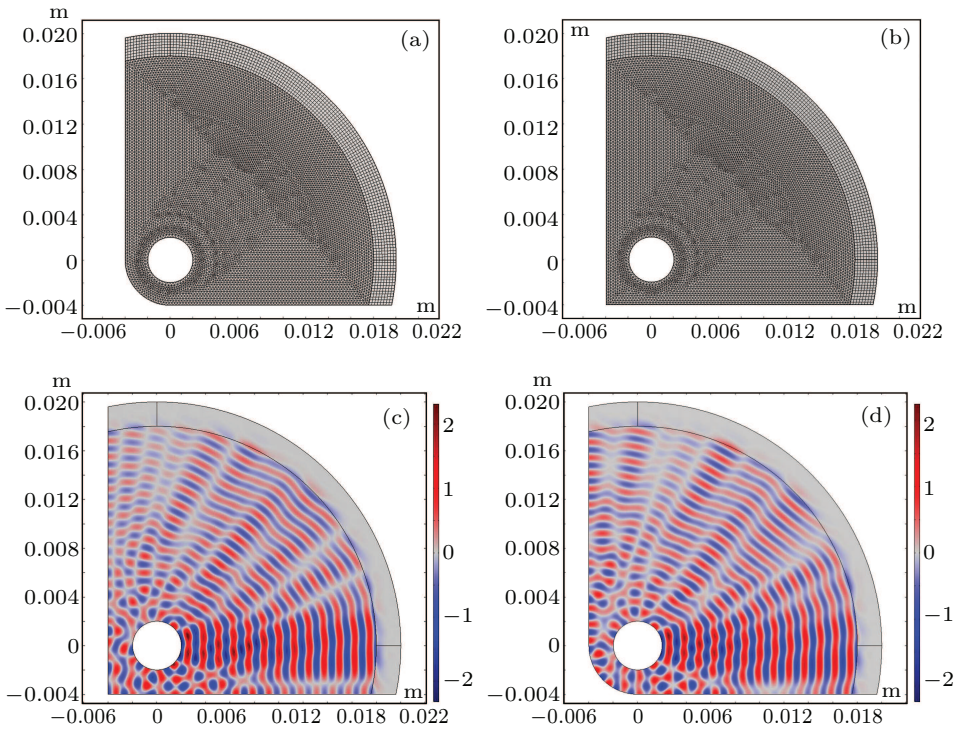


Fig. 15. The numerical models of two types of rigid corners. The angle α between two rigid boundaries is set as 90°, the incident angle φ is set as 0° and the normalized distance $d_1 = d_2 = 2$. (a) The meshes for the right angle rigid corner model. (b) The meshes for the circular rigid corner model. (c) The total acoustic pressure field P_t for the right angle rigid corner model. (d) The total acoustic pressure field P_t for the circular rigid corner model.

Figure 16 exhibits the 2D plots of the acoustic radiation force function components versus ka and w for a rigid cylindrical particle near two types of corners placed in a Gaussian beam field. The color bars of Figs. 16(c) and 16(d) are, respectively, adjusted to the same as in Figs. 16(a) and 16(b) to contrast clearly with other figures. The transformation tendencies of the acoustic radiation force function of two types boundaries are basically the same, but Y_x is weakened and Y_x is enhanced in the circular rigid corner case due to the reflection of the circular boundary. It is feasible to analyze more complex boundaries by changing the parameters of model.

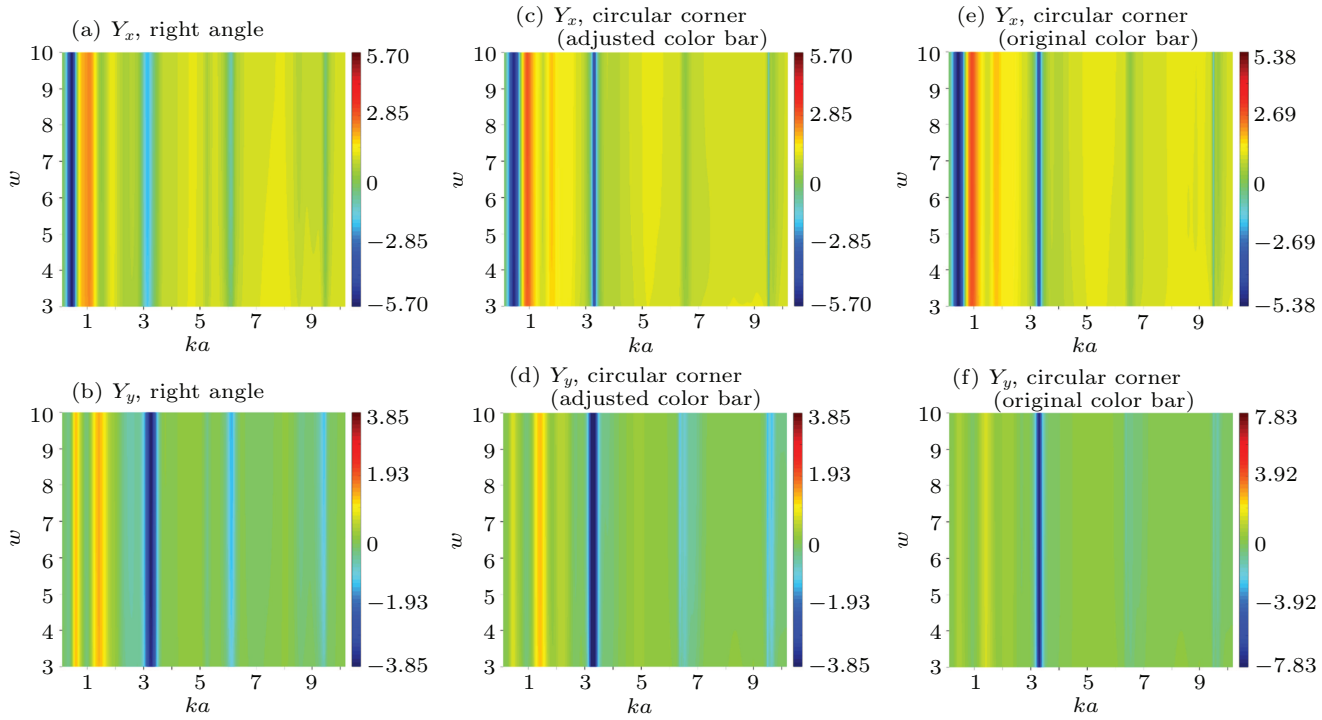


Fig. 16. The 2D plots of the acoustic radiation force function components versus ka and w for a rigid cylindrical particle near two types of rigid corners placed in a Gaussian beam field. The angle α between two rigid boundaries is set as 90°, the incident angle φ is set as 0° and the normalized distance $d_1 = d_2 = 2$. (a) The acoustic radiation force component in the Y direction of the right angle rigid corner. (b) The acoustic radiation force component in the Y direction of the right angle rigid corner. [(c), (e)] The acoustic radiation force component in the X direction of the circular rigid corner. [(d), (f)] The acoustic radiation force component in the Y direction of the circular rigid corner.

4. Conclusions

In summary, an FEM numerical model is presented for the acoustic radiation force exerting on a rigid cylindrical particle immersed in fluid near a rigid corner, which is so difficult to figure out by PWSEM because of the complex reflection from boundaries. Compared with PESEM, FEM is more suitable to calculate the acoustic radiation force existed in intricate geometries.

Numerical simulation shows that the amplitude of the acoustic radiation force function has visible changes at small ka due to ratio of a to λ. The transformation of the acoustic radiation force depends on the generation of standing wave that the tendency is significantly affected by ka and the distance from the center of cylinder to each boundary. When ka decreases, the variation frequency of acoustic radiation force function appears obvious oscillations along with the distance. The positions of the acoustic radiation force function peaks change with ka. This study provides a numerical method to calculate the acoustic radiation force on a particle nearby multiple boundaries and is expected to improve and develop the acoustic particle manipulation in practical applications.

Acknowledgements

This work was supported by the National Natural Science Foundation of China (Grant Nos. 11604361 and 11904384), the National Key R&D Program of China (Grant No. 2018YFC0114900), and Youth Innovation Promotion Association, Chinese Academy of Sciences (Grant No. 2019024).

References

[1] Wu J R 1991 *J. Acoust. Soc.* **89** 2140
[2] Lee J W, Ha K L and Shung K K 2005 *J. Acoust. Soc. Am.* **117** 3273
[3] Yarin A L, Pfaffenlehner M and Troper C 1998 *J. Fluid Mech.* **356** 65
[4] King L V 1934 *Proc. R. Soc. London A* **147** 212
[5] Awatani J 1953 *J. Acous. Soc. Jpn.* **9** 140
[6] Yosioka K 1955 *Acta Acust. United Acust.* **5** 167
[7] Yosioka K, Hasegawa T and Omura A 1969 *Acustica* **22** 145
[8] Hasegawa T and Yosioka K 1969 *J. Acoust. Soc. Am.* **46** 1139
[9] Hasegawa T and Watanabe Y 1978 *J. Acoust. Soc. Am.* **46** 1733
[10] Hasegawa T 1979 *J. Acoust. Soc. Am.* **65** 32
[11] Hasegawa T, Saka K, Inoue N and Matsuzawa K 1988 *J. Acoust. Soc. Am.* **83** 1770
[12] Wu J R and Du G H 1990 *J. Acoust. Soc. Am.* **87** 997
[13] Marston P L 2006 *J. Acoust. Soc. Am.* **120** 3518
[14] Marston P L 2009 *J. Acoust. Soc. Am.* **125** 3539
[15] Mitri F G 2008 *Ann. Phys.* **323** 2840
[16] Mitri F G 2009 *Ultrasonics* **49** 794
[17] Mitri F G 2009 *J. Phys. A: Math. Theor.* **42** 245202
[18] Mitri F G 2009 *Eur. Phys. J. E* **28** 469
[19] Azarpeyvand M 2013 *J. Sound. Vib.* **332** 2338
[20] Wu R R, Cheng K X, Liu X Z, Liu J H and Gong X F 2016 *Wave Motion* **62** 63
[21] Chen J, Liu X Z, Liu J H, Mao Y W and Marston P L 2017 *Ultrasonics* **76** 1
[22] Guanauard G C and Huang H 1994 *J. Acous. Soc. Am.* **96** 2526
[23] Huang H and Guanauard G C 1997 *Int. J. Solids Structures* **34** 591
[24] Miri A K and Mitri F G 2011 *Ultrasound Med. Biol.* **37** 301
[25] Wang J and Dual J 2012 *Ultrasonics* **52** 325
[26] Qiao Y P, Zhang X F and Zhang G B 2017 *J. Acoust. Soc. Am.* **141** 4633
[27] Qiao Y P, Zhang X F and Zhang G B 2017 *Wave Motion* **74** 182
[28] Qiao Y P, Shi T Y, Zhang X F and Zhang G B 2018 *Wave Motion* **83** 111
[29] Qiao Y P, Wang H B, Liu X Z and Zhang X F 2020 *Wave Motion* **93** 102478
[30] Qiao Y P, Zhang X W, Gong M Y, Wang H B and Liu X Z 2020 *J. Appl. Phys* **128** 044902
[31] Zang Y C, Lin W J, Su C and Wu P F 2021 *Chin. Phys. B* **30** 044301
[32] Mitri F G 2014 *Ann. Phys.* **342** 158